Available online at www.sciencedirect.com
ScienceDirect
International Journal of Heat and Mass Transfer 51 (2008) 1402–1408
International Journal of HEAT and MASS TRANSFER
www.elsevier.com/locate/ijhmt

A fractal model for the starting pressure gradient for Bingham fluids in porous media

Meijuan Yun, Boming Yu *, Jianchao Cai

Department of Physics, Huazhong University of Science and Technology, 1037 Luoyu Road, Wuhan 430074, Hubei, PR China

Received 26 October 2007
Available online 31 December 2007

Abstract

In this paper, we present a fractal model for the starting pressure gradient for Bingham fluids in porous media based on the fractal characteristics of pores in the media and on the capillary pressure effect. Every parameter in the proposed models has clear physical meaning, and the proposed model relates the starting pressure gradient of Bingham fluids to the structural parameters of porous media, the yield stress, the capillary pressure parameters and the fractal dimensions of porous media. The model predictions from the present model for the starting pressure gradient are in good agreement with the available expression Eq. (2). The results also show that at smaller radii ($\bar{r} < 0.3$ mm) and low porosity ($\phi < 0.3$), the capillary pressure has the significant influence on the starting pressure gradient in porous media and thus cannot be neglected. However, at high porosity, the starting pressure gradient is primarily produced by the shear stress and the contribution to the starting pressure gradient from the capillary pressure is negligible.

Keywords: Bingham fluids; Porous media; Starting pressure gradient; Fractal; Capillary pressure

1. Introduction

Considerable evidence from laboratory experiments and field tests indicate that certain fluids in porous media exhibit a Bingham-type non-Newtonian behavior [1,2]. The studies of flow behavior for Bingham plastic fluids in porous media have steadily received much attention in the past [3–6]. Typical Bingham fluids include paint, slurries, pastes, food substances, heavy oil as well as foams. Wu et al. [7] presented an integral analysis method for single phase Bingham flow and a Buckley–Leverett type analytical solution for two-phase immiscible displacement with Bingham non-Newtonian fluids. They also developed a numerical model for single- and multi-phase Bingham fluid flow through porous media by suitably modifying a general-purposed multi-phase reservoir simulator. Blackery and Mitsoulis [8] numerically studied the creeping flow of a Bingham plastic around a sphere contained in a cylindrical tube. Roquet and Saramito [9] performed the numerical simulation on the steady flow of a yield stress fluid around a cylinder. Balhoff and Thompson [10] simulated the Bingham fluid flow through axis-symmetrical constricted duct by the finite element method (FEM).

The rheology equation for a Bingham plastic is $\tau = \tau_0 - \mu\dot{\gamma}$ [11], where τ is shear stress, τ_0 is the yield stress which is stress that must be exceeded for flow to begin, μ is the Bingham plastic viscosity and $\dot{\gamma}$ is the shear rate.

Prada and Civan [12] obtained the following empirical correlation for saturated brine through typical sandstones, Brown sandstones and sand-packs as

$$\lambda = 16(K/\mu)^{-0.8} \tag{1}$$

where λ is the starting pressure gradient, and 16 and -0.8 are empirical constants. Eq. (1) indicates that the starting pressure gradient λ is a function of permeability K of a porous medium and the viscosity μ of fluid.

Wang et al. [13] developed a theoretical expression for the starting pressure gradient for heavy oil flow in porous media

* Corresponding author. Tel.: +86 27 87542153.
E-mail address: yuboming2003@yahoo.com.cn (B. Yu).

0017-9310/$ - see front matter © 2007 Elsevier Ltd. All rights reserved.
doi:10.1016/j.ijheatmasstransfer.2007.11.016

$$\lambda = 2\tau_0\left(\frac{\phi}{8K}\right)^{\frac{1}{2}} \tag{2}$$

It can be seen from Eq. (2) that the starting pressure gradient λ is directly proportional to yield stress τ_0 of heavy oil, porosity ϕ and inversely proportional to the permeability of porous media. In Eqs. (1) and (2), the permeability is usually determined by other methods such as numerical solutions and experimental measurements.

Since 1980s, the fractal geometry theory [14] has been used as a tool in many disciplines to characterize irregular or disordered objects [14–16] such as coast lines, clouds and islands, roughness of surfaces, sandstone pores [17,18], fracture surfaces of metal [19], and granular materials [20] etc. The pores and their distributions in porous media are analogous to islands or lakes on earth and to contact spots on engineering surfaces. Therefore, it is possible to model the transport properties such as flow resistance and permeability for flow in porous media by fractal geometry theory. Fractal geometry theory has been proven to be powerful means for analysis of porous media [17,21–25]. In the light of this point, Yu et al. [23,24] proposed a fractal geometry model for permeability of porous media and their model has been shown to be suitable not only for particle porous media [23] but also for porous fabrics [24]. However, their model was for Newtonian fluid and was not involved in the starting pressure gradient for Bingham fluids in porous media.

In this paper, based on the basic fractal characters of microstructures of porous media, a fractal model for the starting pressure gradient for Bingham fluids in porous media, which accounts for the capillary pressure, is derived. The model predictions are then compared with those predicted by the available expression Eq. (2).

2. The basic theory for fractal porous media

It has been shown that the cumulative size distribution of pores in porous media follows the fractal scaling law [23,24]:

$$N(L \geqslant r) = \left(\frac{r_{\max}}{r}\right)^{D_f} \tag{3}$$

where $r_{\max}$ is the maximum pore radius, and D_f is determined by

$$D_f = d_E - \frac{\ln\phi}{\ln(r_{\min}/r_{\max})} \tag{4}$$

where ϕ is porosity, $1 < D_f < 2$ is pore area fractal dimension in two dimensions. Eq. (4) indicates that the pore area fractal dimension increases with the increase of porosity, and D_f approaches its possible maximum value of 2 as porosity ϕ tends to 1. This is consistent with the physical situation because when porosity $\phi = 1$, this means that a plane is completely occupied by pores, leading to the dimension of 2. In Eq. (4), $r_{\min}$ and $r_{\max}$ are the minimum and maximum radii of pores, respectively. In general, the ratio is $r_{\min}/r_{\max} < 10^{-2}$ in porous media.

Differentiating Eq. (3) with respect to r results in the number of pores whose radii are within the infinitesimal range r to $r + dr$,

$$-dN = D_f r_{\max}^{D_f} r^{-(D_f+1)} dr \tag{5}$$

In Eq. (5), $-dN > 0$, which implies the number of pores decreases with the increase of pore size.

The fractal scaling law for the tortuous capillaries in porous media is [25]

$$L = L_0^{D_T}(2r)^{1-D_T} \tag{6}$$

where r is the radius of pore/capillary. L_0 and L are the straight distance and actual length of a tortuous capillary, respectively, and $L \geqslant L_0$. D_T is the fractal dimension for tortuosity, $1 < D_T < 2$ in two dimensions and $1 < D_T < 3$ in three dimensions. The tortuosity fractal dimension decreases with the increase of porosity. $D_T = 1$ represents a straight capillary and $L = L_0$. When porosity is unity, this implies that there is no solid particle in a volume and the streamlines are straight and thus $D_T = 1$. A higher value of D_T corresponds to a highly tortuous capillary. $D_T = 2$ and $D_T = 3$ correspond to a so highly tortuous line that fills a two-dimensional plane and a three-dimensional space, respectively. Eq. (6) also shows that the larger the capillary r, the shorter the capillary length L. This is consistent with the physical situation.

For a given capillary (i.e. keep r unchanged), differentiating Eq. (6) yields

$$dL = L_0^{D_T-1}(2r)^{1-D_T} D_T dL_0 \tag{7}$$

The structural parameters for porous media are [23]

$$L_0 = \bar{r}\sqrt{\frac{2\pi}{\sqrt{3}(1-\phi)}} \tag{8}$$

and

$$r_{\max} = \frac{\bar{r}}{4}\left[\sqrt{\frac{2\phi}{1-\phi}} + \sqrt{\frac{2\pi}{\sqrt{3}(1-\phi)}} - 2\right] \tag{9}$$

In Eqs. (8) and (9), $\bar{r}$ is the average radius of particles in porous media.

The fractal dimension D_T for tortuous capillaries in porous media can be expressed as [25]

$$D_T = 1 + \frac{\ln\Gamma}{\ln\frac{L_0}{2r_{av}}} \tag{10}$$

where Γ and r_{av} are the average tortuosity (defined by $\Gamma = L/L_0$) of tortuous capillaries and the average pore radius, respectively.

A correlation between the average tortuosity of flow path was given by [26]

$$\Gamma = 1 + 0.41\ln(1/\phi) \tag{11}$$

which was obtained by the experiments on flow through beds packed with spherical particles.

In porous media, the pore sizes are non-uniform. Kong [27] gives the average pore radius

$$r_{av} = \left(\sum_{i=1}^{N} N_i r_i^4\right)^{\frac{1}{4}} \tag{12}$$

where N_i ($i = 1, 2, \ldots, N$) is the number of the capillaries with the radius r_i. Usually, N_i is unknown and the average pore radius cannot be found directly from Eq. (12). However, due to Eq. (5), the average pore radius can be calculated from

$$\begin{aligned} r_{av} &= \left(-\int_{r_{min}}^{r_{max}} r^4 \, dN\right)^{1/4} \\ &= r_{max}\left(\frac{D_f}{4-D_f}\right)^{1/4}\left[1-\left(\frac{r_{min}}{r_{max}}\right)^{4-D_f}\right]^{1/4} \end{aligned} \tag{13}$$

where $1 < D_f < 2$ in the two-dimensional space, $4 - D_f > 2$, $r_{min}/r_{max} < 10^{-2}$, so $(r_{min}/r_{max})^{4-D_k} \ll 1$. Then Eq. (13) can be reduced to

$$r_{av} = r_{max}\left(\frac{D_f}{4-D_f}\right)^{1/4} \tag{14}$$

Eq. (14) presents a fractal model for the average pore radius in porous media.

3. Fractal models for the starting pressure gradient with capillary pressure included for Bingham fluids in porous media

The flow rate through a single capillary for Bingham fluids is given by [11]

$$\begin{aligned} q &= \frac{\pi r^4}{8\mu}\left(-\frac{dp}{dL}\right)\left[1-\frac{4}{3}\left(\frac{2\tau_0/r}{-dp/dL}\right)+\frac{1}{3}\left(\frac{2\tau_0/r}{-dp/dL}\right)^4\right] \\ &= \frac{\pi r^4}{8\mu}\left(-\frac{dp}{dL}\right)\left[\left(1-\frac{2\tau_0/r}{|-dp/dL|}\right)\right. \\ &\quad \left.-\frac{1}{3}\frac{2\tau_0/r}{|-dp/dL|}\left(1-\frac{(2\tau_0/r)^3}{|-dp/dL|^3}\right)\right] \end{aligned} \tag{15}$$

In Eq. (15), the starting pressure gradient $\lambda = \frac{2\tau_0}{r}$ is obtained when we let $q = 0$. For simplicity, according to the same approximate method as that in derivation of generalized Darcy's law for Bingham fluids [27], we keep the first term in the square bracket in Eq. (15) and omit the second term. Then Eq. (15) can be reduced to

$$q = \frac{\pi r^4}{8\mu}\left(-\frac{dp}{dL}\right)\left(1-\frac{2\tau_0/r}{|-dp/dL|}\right) \tag{16}$$

Eq. (16) still satisfies the flow rate $q = 0$ when $|dp/dL| = \lambda$.

For plane-parallel flow, the pressure p decreases with the increase of the length L, so $dp/dL < 0$, Eq. (16) can be rewritten as

$$q = \frac{\pi r^4}{8\mu}\left(-\frac{dp}{dL}\right)\left(1+\frac{2\tau_0/r}{dp/dL}\right) \tag{17}$$

Because of the fractal characteristics of tortuous capillary/streamline, inserting Eq. (7) into Eq. (17) yields

$$q(r) = \frac{\pi \cdot r^4 \Delta p}{8\mu D_T L_0}\left(\frac{L_0}{2r}\right)^{1-D_T} - \frac{\pi \cdot r^3 \tau_0}{4\mu} \tag{18}$$

If the capillary pressure p_c is taken into account, Eq. (18) can be rewritten as

$$q(r) = \frac{\pi \cdot r^4 (\Delta p + \Delta p_c)}{8\mu D_T L_0}\left(\frac{L_0}{2r}\right)^{1-D_T} - \frac{\pi \cdot r^3 \tau_0}{4\mu} \tag{19}$$

where $\Delta p_c < 0$ when the capillary pressure blocks the fluid flow through tortuous capillaries; otherwise $\Delta p_c > 0$.

The capillary pressure difference is given by [28]

$$\Delta P_c = \frac{F\sigma\cos\theta}{2r}\frac{1-\phi}{\phi} \tag{20}$$

In Eq. (20), σ is surface tension of wetting fluid, θ is contact angle between liquid and solid, and F is shape factor depending on geometry of a medium and on flow direction.

It has been shown that the pore size distribution in porous media follows the fractal power law, so the total flow rate Q through the cross-section can be obtained by integrating Eq. (19) over the entire range of pore sizes

$$\begin{aligned} Q &= -\int_{r_{min}}^{r_{max}} q(r)\, dN(r) \\ &= \frac{\pi D_f r_{max}^{D_f} \Delta p}{8\mu L_0^{D_T} 2^{1-D_T} D_T (D_T - D_f + 3)} r_{max}^{D_T - D_f + 3}\left[1-\left(\frac{r_{min}}{r_{max}}\right)^{3+D_T-D_f}\right] \\ &\quad + \frac{\pi F\sigma\cos\theta(1-\phi)D_f r_{max}^{2+D_T}}{2^{5-D_T}\mu D_T L_0^{D_T}\phi(2+D_T-D_f)}\left[1-\left(\frac{r_{min}}{r_{max}}\right)^{2+D_T-D_f}\right] \\ &\quad - \frac{\pi\tau_0 D_f r_{max}^{D_f}}{4\mu(3-D_f)} r_{max}^{3-D_f}\left[1-\left(\frac{r_{min}}{r_{max}}\right)^{3-D_f}\right] \end{aligned} \tag{21}$$

In general, $r_{min}/r_{max} < 10^{-2}$ in porous media, and $1 < D_T < 2$, $1 < D_f < 2$ in two dimensions, $3 + D_T - D_f > 1$, $2 + D_T - D_f > 1$ and $3 - D_f > 1$, so $\left(\frac{r_{min}}{r_{max}}\right)^{3+D_T-D_f} \ll 1$, $\left(\frac{r_{min}}{r_{max}}\right)^{2+D_T-D_f} \ll 1$ and $\left(\frac{r_{min}}{r_{max}}\right)^{3-D_f} \ll 1$. It follows that Eq. (21) can be reduced to

$$\begin{aligned} Q &= \frac{\pi D_f r_{max}^{3+D_T}}{8\mu L_0^{D_T-1} 2^{1-D_T} D_T (3+D_T-D_f)} \\ &\quad \times\left[\frac{\Delta p}{L_0} + \frac{F\sigma\cos\theta(1-\phi)(3+D_T-D_f)}{2L_0\phi(2+D_T-D_f)r_{max}}\right. \\ &\quad \left.- \frac{L_0^{D_T-1} D_T (3+D_T-D_f)\tau_0}{2^{D_T-2}(3-D_f) r_{max}^{D_T}}\right] \end{aligned} \tag{22}$$

The total cross-sectional area of porous media is

$$A = \frac{A_p}{\phi} = \frac{-\int_{r_{min}}^{r_{max}} \pi r^2 \, dN}{\phi} = \frac{\pi D_f}{\phi(2-D_f)} r_{max}^2 \left[1 - \left(\frac{r_{min}}{r_{max}}\right)^{2-D_f}\right] \quad (23)$$

where A_p is the total pore area of a cross-section.

The porosity is related to the fractal dimension for pore spaces and microstructural parameters by [29]

$$\phi = \left(\frac{r_{min}}{r_{max}}\right)^{2-D_f} \quad (24)$$

Substituting Eq. (24) into Eq. (23), we obtain

$$A = \frac{\pi D_f}{\phi(2-D_f)} r_{max}^2 (1-\phi) \quad (25)$$

Dividing Eq. (22) by Eq. (25) gives the average (superficial) velocity for Bingham fluids in porous media

$$V = \frac{r_{max}^{1+D_T}\phi(2-D_f)}{\mu L_0^{D_T-1} 2^{4-D_T} D_T(3+D_T-D_f)(1-\phi)} \times \left[\frac{\Delta p}{L_0} + \frac{F\sigma\cos\theta(1-\phi)(3+D_T-D_f)}{2L_0\phi(2+D_T-D_f)r_{max}} - \frac{L_0^{D_T-1} D_T(3+D_T-D_f)\tau_0}{2^{D_T-2}(3-D_f) r_{max}^{D_T}}\right] \quad (26)$$

When the yield stress $\tau_0 = 0$, the fluid becomes Newtonian. According to Eqs. (22) and (26), and we can obtain the flow rate and velocity for Newtonian fluids with capillary pressure included:

$$Q = \frac{\pi D_f r_{max}^{3+D_T}}{8\mu L_0^{D_T-1} 2^{1-D_T} D_T(3+D_T-D_f)} \times \left[\frac{\Delta p}{L_0} + \frac{F\sigma\cos\theta(1-\phi)(3+D_T-D_f)}{2L_0\phi(2+D_T-D_f)r_{max}}\right] \quad (27)$$

$$V = \frac{r_{max}^{1+D_T}\phi(2-D_f)}{\mu L_0^{D_T-1} 2^{4-D_T} D_T(3+D_T-D_f)(1-\phi)} \times \left[\frac{\Delta p}{L_0} + \frac{F\sigma\cos\theta(1-\phi)(3+D_T-D_f)}{2L_0\phi(2+D_T-D_f)r_{max}}\right] \quad (28)$$

In Eqs. (27) and (28), the term $\frac{F\sigma\cos\theta(1-\phi)(3+D_T-D_f)}{2L_0\phi(2+D_T-D_f)r_{max}}$ is also called the starting pressure gradient if the contact angle $\theta > \pi/2$, and this means that the starting pressure gradient also exists for Newtonian fluid flow in porous media as the contact angle $\theta > \pi/2$.

Let $Q = 0$ in Eq. (22) or $V = 0$ in Eq. (26), the starting pressure gradient for Bingham fluids in porous media is obtained as follows:

$$\lambda = \frac{L_0^{D_T-1} D_T(3+D_T-D_f)\tau_0}{2^{D_T-2}(3-D_f) r_{max}^{D_T}} - \frac{F\sigma\cos\theta(1-\phi)(3+D_T-D_f)}{2L_0\phi(2+D_T-D_f)r_{max}} = \lambda_1 - \lambda_2 \quad (29)$$

where $\lambda_1 = \frac{L_0^{D_T-1} D_T(3+D_T-D_f)\tau_0}{2^{D_T-2}(3-D_f) r_{max}^{D_T}}$ (30)

$$\lambda_2 = \frac{F\sigma\cos\theta(1-\phi)(3+D_T-D_f)}{2L_0\phi(2+D_T-D_f)r_{max}} \quad (31)$$

Eq. (29) is the fractal analytical model for the starting pressure gradient for Bingham fluids flow in porous media, in which the capillary pressure effect is taken into account. Eq. (30) represents the starting pressure gradient contribution from the shear stress, and Eq. (31) denotes the starting pressure gradient contribution from the capillary pressure. It is seen from Eq. (29) that the starting pressure gradient λ is related not only to the yield stress τ_0 but also to the structural parameters of porous media (D_T, D_f, L_0 and r_{max}) as well as the capillary pressure parameters (σ, F and θ). Though Eqs. (1) and (2) appear simple, they have an unknown permeability and do not include the effect of capillary pressure, microstructural parameters on the starting pressure gradient. Therefore, the present model Eq. (29) clearly reveals the physical mechanisms for the starting pressure gradient for Bingham fluids in porous media.

4. Comparisons

This section is devoted to verifying the validity of the proposed model by comparisons with the available expressions. The parameters D_f, L_0, r_{max} and D_T in Eq. (29) are determined by Eqs. (4), (8), (9) and (10), respectively. $\tau_0 = 0.1$, $F = 4$ [28] and $\sigma = 0.044\ N.m$, $\theta = 57^0$ [30] are used in Eq. (29) in the present comparisons.

The permeability K of porous media in Eq. (2) are calculated by the follow fractal permeability expression [31]

$$K = 2^{D_T-4}\frac{\phi L_0^{1-D_T}}{D_T}\frac{(2-D_f)r_{max}^{1+D_T}}{(D_T-D_f+3)(1-\phi)} \quad (32)$$

Figs. 1–3 compare fractal model predictions by Eq. (30) with Eq. (2) [13] for the starting pressure gradient contribution from the shear stress for Bingham fluid flow in porous media at different porosities, radii and yield stresses, respectively. It is seen that good agreement between the two models is obtained, and this verifies the validity of the proposed fractal model Eq. (30).

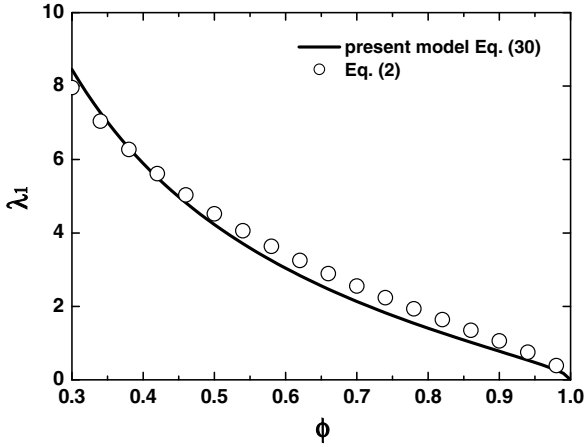

Fig. 1. The starting pressure gradient contribution from shear stress versus porosity between the present model Eqs. (30) and (2) [13].

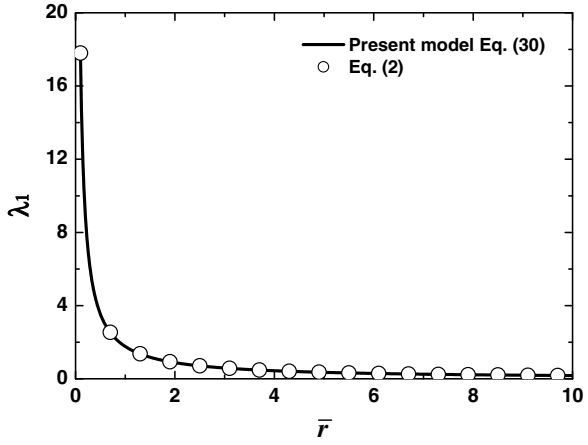

Fig. 2. The starting pressure gradient contribution from shear stress versus the radius of particles between the present model Eqs. (30) and (2) [13].

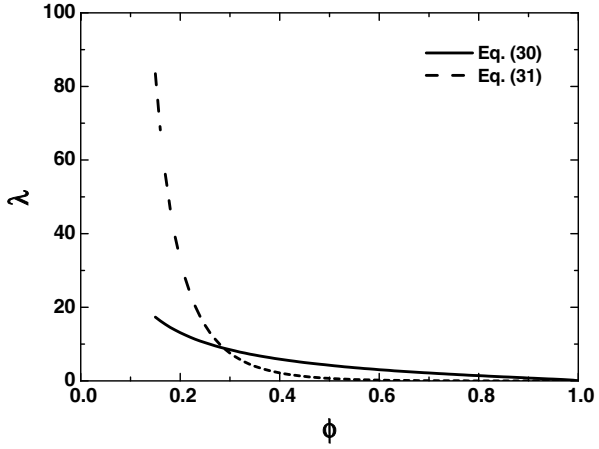

Fig. 4. The starting pressure gradient versus the porosity between Eq. (30) contribution from shear stress and Eq. (31) contribution from capillary pressure.

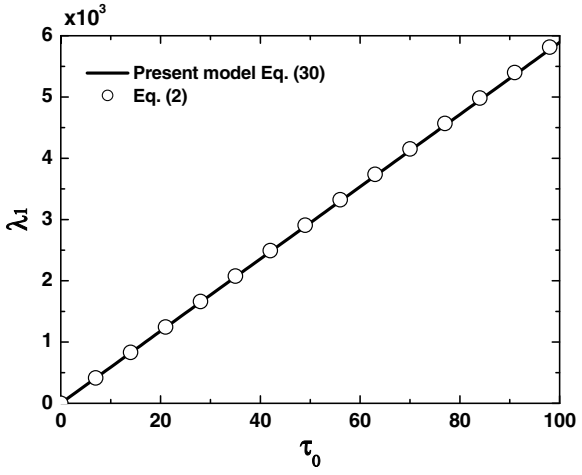

Fig. 3. The starting pressure gradient contribution from shear stress versus yield stress between the present model Eqs. (30) and (2) [13].

When the average radius ($\bar{r} = 0.3$ mm) of particles keeps unchanged, Fig. 4 compares the starting pressure gradient contributions from the shear stress by Eq. (30) and that from the capillary pressure by Eq. (31), respectively. The figure shows that the starting pressure gradient contribution λ_2 from the capillary pressure decreases rapidly with the increase of porosity, and $\lambda_2 \to 0$ when $\phi > 0.6$. Therefore, the effect of capillary pressure on the starting pressure gradient can be neglected at high porosity. However, at low porosity, the capillary pressure has the significant influence on the starting pressure gradient, and this reveals that the capillary pressure may be an important physical mechanism for the starting pressure gradient in porous media at low porosity. This may be interpreted as that at low porosity, the diameters of capillaries become very small, and the molecular force may dominate the resistance for flow and thus cause the flow resistance increase drastically. This, therefore, may need the larger starting pressure gradient to drive the flow in porous media at low porosity than at high porosity.

Fig. 5 again compares the starting pressure gradient contributions from the shear stress by Eq. (30) and that from the capillary pressure by Eq. (31) at different porosities and at different particle sizes. We can see from Fig. 5 that the starting pressure gradients from both the shear stress (λ_1) and from the capillary pressure (λ_2) decrease rapidly with the increase of radii of particles, and the contribution from the capillary pressure may be much less than that from the shear stress when $\bar{r} > 0.4$ mm. Therefore, the effect of capillary pressure on the starting pressure gradient may be neglected at larger radii of particles. However, at smaller radii ($\bar{r} < 0.3$ mm) and low porosity ($\phi < 0.3$) (see Figs. 5a and b), the capillary pressure has the significant influence on the starting pressure gradient in porous media and thus cannot be neglected. This phenomenon may be explained that the smaller radii of particles in a porous medium with usually correspond to the smaller pore sizes, leading to the higher capillary pressure and higher starting pressure gradient. However, at high porosity the starting pressure gradient from the shear stress is much larger than that from the capillary pressure, see Fig. 5c. This implies that at high porosity the starting pressure gradient is primarily produced by the shear stress.

The present model for the starting pressure gradient in porous media is analytically related to the yield stress τ_0, the structural parameters (L_0 and r_{max}), the capillary pressure parameters (σ, F and θ) and the fractal dimensions (D_T and D_f), and the physical principles are fully revealed. However, the conventional models such as Eqs. (1) and (2) contain one or more empirical constants with no physical meaning, and these models cannot fully reveal the underlying physical mechanisms for the starting pressure gradient in porous media. In addition, in the conventional methods, the permeability needs to be solved by experiments or numerical simulations or by other empirical correlations. Whereas there is no empirical constant and every parameter in the proposed model has specific physical significance, and the starting pressure gradient based on the

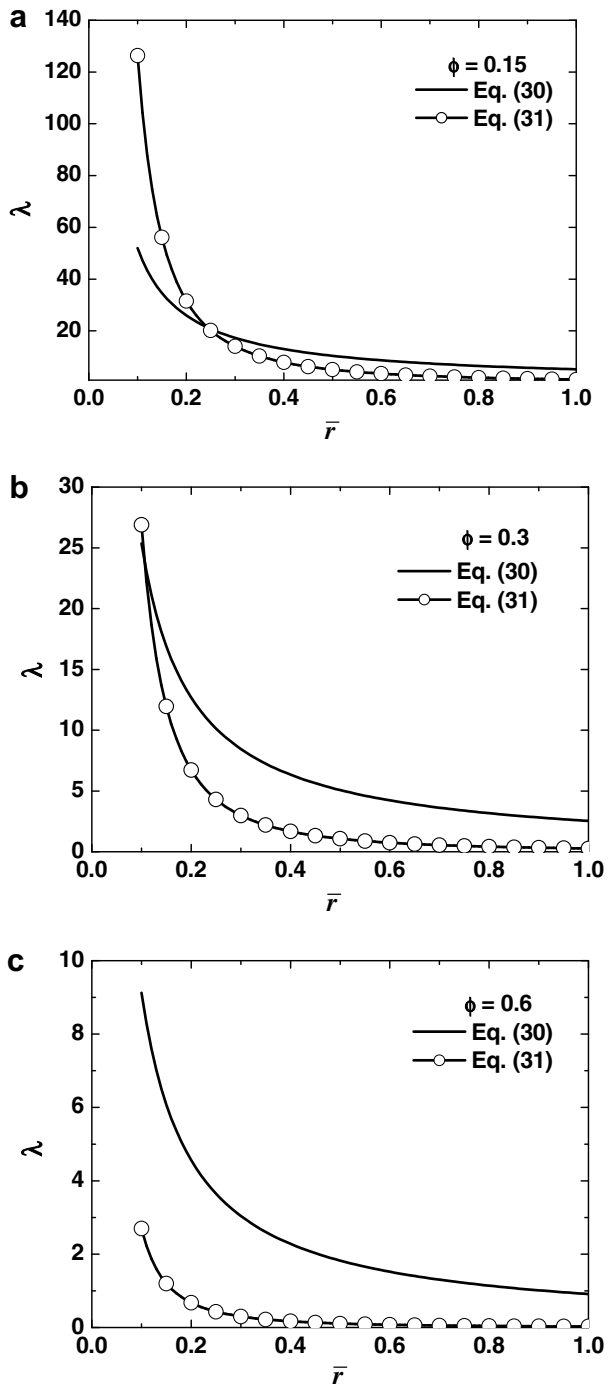

Fig. 5. The starting pressure gradient versus the radius of particles between Eq. (30) contribution from shear stress and Eq. (31) contribution from capillary pressure. (a) $\phi = 0.15$, (b) $\phi = 0.3$, and (c) $\phi = 0.6$.

fractal geometry theory is directly expressed as a function of the microstructural parameters of porous media and properties of fluid.

5. Conclusions

We have shown the fractal model for the starting pressure gradient for Bingham fluid flow in porous media. The proposed model accounts for the effects of the shear stress and capillary pressure on the starting pressure gradient. Every parameter in the proposed fractal model has clear physical meaning. The proposed model relates the starting pressure gradient of Bingham fluids in porous media to the structural parameters of porous media, the yield stress, the capillary pressure parameters and the fractal dimensions of porous media. While conventional models cannot fully reveal the physical mechanisms for the starting pressure gradient in porous media. The present results show that at smaller radii ($\bar{r} < 0.3$ mm) and low porosity ($\phi < 0.3$), the capillary pressure has the significant influence on the starting pressure gradient in porous media and thus cannot be neglected. However, at high porosity the starting pressure gradient is primarily produced by the shear stress and the contribution to the starting pressure gradient from the capillary pressure is negligible.

Acknowledgement

This work was supported by the National Natural Science Foundation of China through Grant Number 10572052.

References

[1] J. Bear, Dynamics of Fluids in Porous Media, Elsevier, New York, 1972.
[2] G.E. Barenblatt, B.M. Entov, B.M. Rizhik, Flow of Liquids and Gases in Natural Formations, Nedra, Moscow, 1984.
[3] G.C. Vradis, J. Dougher, S. Kumar, Entrance pipe flow and heat transfer for a Bingham plastic, Int. J. Heat Mass Transfer 36 (1993) 543–552.
[4] K.J. Hammad, G.C. Vradis, Creeping flow of a Bingham plastic through axisymmetric sudden contractions with viscous dissipation, Int. J. Heat Mass Transfer 39 (1996) 1555–1567.
[5] U.C.S. Nascimento, E.N. Macêdo, J.N.N. Quaresma, Thermal entry region analysis through the finite integral transform technique in laminar flow of Bingham fluids within concentric annular ducts, Int. J. Heat Mass Transfer 45 (2002) 923–929.
[6] R. Khatyr, D. Ouldhadda, A. Il Idrissi, Viscous dissipation effects on the asymptotic behaviour of laminar forced convection for Bingham plastics in circular ducts, Int. J. Heat Mass Transfer 46 (2003) 589–598.
[7] Y.S. Wu, K. Pruess, P.A. Witherspoon, Flow and displacement of Bingham non-Newtonian fluids in porous media, SPERE 7 (1992) 369–376.
[8] J. Blackery, E. Mitsoulis, Creeping motion of a sphere in tubes filled with a Bingham plastic material, J. Non-Newton. Fluid Mech. 70 (1997) 59–77.
[9] N. Roquet, P. Saramito, An adaptive finite element method for Bingham fluid flows around a cylinder, Comput. Meth. Appl. Mech. Eng. 192 (2003) 3317–3341.
[10] M.T. Balhoff, K.E. Thompson, Modeling the steady flow of yield-stress fluids in packed beds, AICHE J. 50 (2004) 3034–3048.
[11] R.B. Bird, W.E. Stewart, E.N. Lightfoot, Transport Phenomena, Wiley, New York, 1960.
[12] A. Prada, F. Civan, Modification of Darcy's law for the threshold pressure gradient, J. Petrol. Sci. Eng. 22 (1999) 237–240.
[13] S.J. Wang, Y.Z. Huang, F. Civan, Experimental and theoretical investigation of the Zaoyuan field heavy oil flow through porous media, J. Petrol. Sci. Eng. 50 (2006) 83–101.
[14] B.B. Mandelbrot, The Fractal Geometry of Nature, Freeman, New York, 1982.

[15] J. Feder, Fractals, Plenum Press, New York, 1988.
[16] J. Feder, A. Aharony, Fractals in Physics, North-Holland, 1989.
[17] A.J. Katz, A.H. Thompson, Fractal sandstone pores: implications for conductivity and pore formation, Phys. Rev. Lett. 54 (1985) 1325–1328.
[18] C.E. Krohn, A.H. Thompson, Fractal sandstone pores: automated measurements using scanning-electron-microscope images, Phys. Rev. B 33 (1986) 6366–6374.
[19] B.B. Mandelbrot, D.E. Passoja, A.J. Paullay, Fractal character of fracture surfaces of metals, Nature 308 (1984) 721–722.
[20] H. Xie, R. Bhaskar, J. Li, Generation of fractal models for characterization of pulverized materials, Miner. Metall. Process. (1993) 36–42.
[21] G. Bayles, G. Klinzing, S. Chiang, Fractal mathematics applied to flow in porous systems, Part. Part. Syst. Char. 6 (1989) 168–175.
[22] J.S. Wu, B.M. Yu, A fractal resistance model for flow through porous media, Int. J. Heat Mass Transfer 50 (2007) 3925–3932.
[23] B.M. Yu, P. Cheng, A fractal model for permeability of bi-dispersed porous media, Int. J. Heat Mass Transfer 45 (2002) 2983–2993.
[24] B.M. Yu, L.J. Lee, H.Q. Cao, A fractal in-plane permeability model for fabrics, Polym. Compos. 22 (2002) 201–221.
[25] B.M. Yu, Fractal character for tortuous streamtubes in porous media, Chin. Phys. Lett. 22 (2005) 158–160.
[26] J. Comiti, M. Renaud, A new model for determining mean structure parameters of fixed beds from pressure drop measurements, Chem. Eng. Sci. 44 (1989) 1539–1545.
[27] X.Y. Kong, Advanced Mechanics of Fluids in Porous Media, Press of University of Science and Technology of China, Hefei, China, 1999.
[28] K.J. Ahn, J.C. Seferis, J.C. Berg, Simultaneous measurements of permeability and capillary pressure of thermosetting matrices in woven fabric reinforcements, Polym. Compos. 12 (1991) 146–152.
[29] B.M. Yu, J.H. Li, Some fractal characters of porous media, Fractals 9 (2001) 365–372.
[30] S. Amico, C. Lekakou, An experimental study of the permeability and capillary pressure in resin-transfer moulding, Comp. Sci. Technol. 61 (2001) 1945–1959.
[31] B. Zhang, B.M. Yu, H.X. Wang, M.J. Yun, A fractal analysis of permeability for power-law fluids in porous media, Fractals 14 (2006) 171–177.